Journal of Molecular Liquids 306 (2020) 112948

Contents lists available at ScienceDirect

Journal of Molecular Liquids

journal homepage: www.elsevier.com/locate/molliq

Striking analogies and dissimilarities between graphene oxides and humic acids: pH-dependent charging and colloidal stability

Etelka Tombácz *[,1], Ildikó Y. Tóth [2], Krisztina Kovács, Erzsébet Illés , Márta Szekeres, Balázs Barna [2], Attila Csicsor [3], Tamás Szabó *

Department of Physical Chemistry and Materials Science, University of Szeged, Rerrich Béla tér 1, Szeged H-6720, Hungary

ARTICLE INFO

Article history:
Received 2 February 2020
Received in revised form 18 March 2020
Accepted 19 March 2020
Available online 20 March 2020

Keywords:
Humic substances
Graphene oxide
Particle aggregation
Salt tolerance
Surface charging
Acidic dissociation

ABSTRACT

This study provides a comparative framework on the elucidation of analogies and differences in the interfacial protolytic processes and the associated colloidal behaviour of a typical humic acid (HA) and a set of single-layer graphene oxide (SLGO) and (multi-layered) graphite oxide samples in aqueous electrolyte media. The pH dependence of the surface charge densities of HA and SLGO was explored at three different salt concentrations by potentiometric acid-base titration, along with simultaneous determination of zeta potential and hydrodynamic sizes. Charging curves obtained in the pH range of 3 to 10 by cyclic titrations reveal the presence of a small hysteresis, proving the chemical stability of SLGO and graphite oxides in weakly acidic and alkaline solutions. HA and SLGO display a parallel shift of the pH-dependencies of their negative charge densities with increasing ionic strength, demonstrating a unique combination of particle and polyelectrolyte-like behaviour, which is absent for multi-layered graphite oxide exhibiting charging curves that resemble to "classical" colloidal particles. An accurate purification of SLGO results in inherent change in its surface properties; however, the salt tolerance of aqueous HA solutions is still superior to that of SLGO dispersions.

1. Introduction

Ubiquitous soil organic matter and the recently highlighted graphene-based materials constitute, according to the contemporary scientific consideration, very different classes of materials. However, a remarkable linkage between them stems from their formation process, which is most often related to chemical oxidation. The oxidation of graphite by strong oxidants in harsh acidic environment (mainly Brodie [1] and Hummers [2] methods and their modifications) leads to the formation of graphite oxide (GO), which is the direct precursor of single-layer graphene oxide (SLGO). On the contrary, humic substances (HS) naturally form from coal by atmospheric oxidation [3] or from dead plant matter through oxidative microbial degradation of organic tissues to "monomers" of poorly definable structure, followed by the polymerization of these monomeric substances into high molecular weight compounds [4]. Their structure and origin have been poorly understood and were always subject to dispute [5]. Despite their commonly established polymeric nature, their basic properties such as elemental composition, molecular weight, or the types and amounts of moieties vary widely [5]. HS are inherently heterogeneous materials both in chemical and in structural points of view; the fractionation of HS extracted from various sources (e.g., soil, coal, peat) is generally accepted and operationally defined. The fractions obtained based on their solubility in water as a function of pH are fulvic acids (FA – soluble at all pHs), humic acids (HA – precipitate below pH ~1) and humins (HMN, not soluble at all) [6].

In 1937, Thiele published a paper on the ion exchange properties of graphite oxide (GO), in which he mentioned that, with alkaline oxidizing agents, HA can be obtained under special conditions as an intermediate stage of the oxidation of graphite [7], pointing out the theoretical possibility for the conversion of "*Graphitsäure*" (meaning "graphitic acid", one of the old names of graphite oxide) into HA. This potential was also suggested by Dimiev et al. [8] but by a different means: transformation into HA-like structures by degradation of GO flakes over prolonged exposure to water. The opposite pathway, that is, the synthesis of few-layer graphene oxide from HA has been published recently by Huang et al. [9]. However, they failed to confirm the typical layered structure of the "HA-converted GO" as indicated by the absence of the characteristic reflection at basal spacings of ca. 6 Å. Therefore, apart from a study on the dispersibility of HA, lignin and graphitic acids

* Corresponding authors.
E-mail addresses: tombacz@chem.u-szeged.hu (E. Tombácz), sztamas@chem.u-szeged.hu (T. Szabó).
[1] Present addresses: Department of Food Engineering, University of Szeged, Moszkvai krt. 5-7, Szeged H-6725, Hungary; Pannon University, Egyetem u. 10, Veszprém H-8200, Hungary.
[2] Present address: Department of Applied and Environmental Chemistry, University of Szeged, Rerrich Béla tér 1, Szeged H-6720, Hungary.
[3] Present address: Hymato Products Ltd., Szentkirályszabadja, Kossuth u 33, H-8225, Hungary.

https://doi.org/10.1016/j.molliq.2020.112948

published several years later than Thiele's note [10], it seems that no experimental work was reported in the past 80 years, regarding the exploration of the analogous behaviour of natural HA and manmade graphite oxide and its exfoliated derivative, SLGO. Based on our long-standing experience on the colloidal behaviour of HS [11,12] and GO [13–15], we discovered that, by evaluating the pH-dependent charging and colloidal stability of a SLGO sample, striking analogies and peculiarities exist between GO and HA, particularly with those of coal origin.

GO and HA have a similarly ill-defined polycondensed, partially aromatic ring-system skeleton with ionic moieties. The polyionic structure emerges in pH-dependent protonation/deprotonation of the O-containing aliphatic and phenolic groups such as hydroxyls and carboxyls. The mainly anionic nature of humic acids and graphene oxides at neutral and basic pHs makes both appropriate for binding inorganic and organic cationic pollutants in either natural or waste waters [16,18–20]. These functional groups are also exploited in chemical modification of graphene oxides for applications in diverse technological, biotechnical and biomedical processes [21–27]. Other O-containing groups (e.g., keto, carbonyl, ester and ether), enhance their hydrophilicity and dissolution in aqueous media. Fig. 1 represents the relative H/C and O/C ratio of SLGO as compared to organic compounds with several compound classes represented by circles overlain on the graph (A) and to humic materials (B) and the generalized structure of HA (C) and GO (D,E) with the O-containing functional groups.

Humic acids and graphene oxide are, therefore, quite similar in their chemical composition, but achieve this state in opposite processes. In the natural formation of HA, organic matter condenses to develop a partially aromatic skeleton from small molecules as precursors. In the artificial production of SLGO, the graphene layers of precursor graphite, which originally contain a fully aromatic, condensed ring system, lose part of their aromatic structure and obtain a similarly partially aromatic skeleton as that of HA. Since both processes take place in oxidative conditions, the O-containing functionality of HA and SLGO should also be greatly similar. Oxidation of graphite generates oxidative debris (or FA) [28] that should be removed by washing. During the purification of SLGO from oxidative debris we also experienced [15] very similar pH-dependent behaviour as in the separation of HA from FA occurring in the natural mixture of HS. The removal of low molecular weight

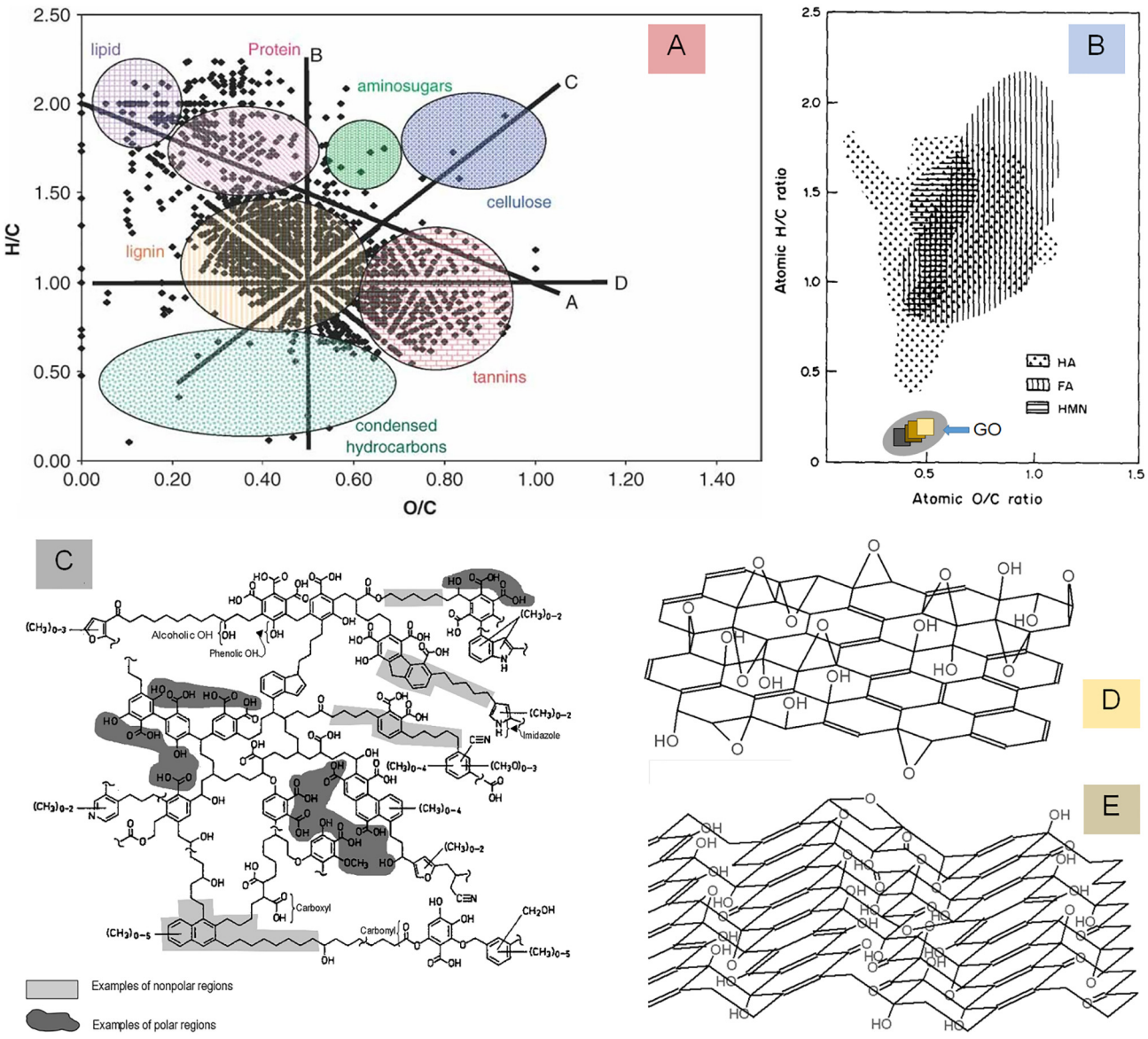

Fig. 1. (A) The H/C vs. O/C (Van Krevelen) diagrams of organic compounds [30,31] and (B) humic substances [32] with data points of a series of GO overlain on the diagram based on our previous publication [13]. (C) The O-containing acidic groups of the carbon skeleton of HS developing charges in pH-dependent dissociation [33] and (D) the Lerf-Klinowski structural model of GO [34,35] in comparison with (E) the structural motives proposed by Szabó et al. [36]. A was reproduced from [31] and C was reproduced from [33] with permission from John Wiley and Sons. B was reproduced from [32] with permission of Elsevier. D was reproduced from [36] with permission of ACS.

components decreased the total acidity and enhanced the pH threshold of aqueous solubility of both materials. The similarity between HS and GO can also be expected based on the work of Dong and co-workers [29] detecting carbon-based nanostructures in the structure of humic acids of different origin, river, peat, soil and a Leonardite sample.

The importance of reactive, mainly oxygen containing groups on the aromatic skeleton in both HA and SLGO in defining their hydrophilicity, pH-dependent charging, and reactions with metal ions both in aqueous phase and at solid interfaces dictates that well-defined potentiometric experiments must be carried out in order to correctly characterize their charging behaviour [13–15]. Unfortunately, several works have already misinterpreted charging or cation complexation of SLGO and used inadequate modelling not relying on its exact chemical speciation and colloidal properties [37,38]. First, the net proton consumption data are not suitable for, and the titration curve in [37] measured only at a single concentration of background electrolyte is not enough to i) determine the pH_{PZC} [39] and ii) model surface protonation processes to calculate intrinsic acidity constants. This incorrect use of fitting software (Fiteql 3.1) leads to the strange conclusion about the formation of positively charged sites on GO nanosheets. Regarding the study of Gu et al. [38], four acidic sites on multilayered GO were supposed for metal ion complexation. Surface complexation modelling of pH-dependent adsorption data of several metal ions seems to be a fitting exercise searching for the best-fitting model involving all or only some of the binding sites. This practice resulted in either non-converging simulations in several cases or larger differences in stability constants calculated at different concentrations of metal ions.

In this work, we present the comparative study of the pH- and ionic strength dependent charge formation and colloidal stability of HA and GO in aqueous solutions. Potentiometric acid-base titration was used to quantify the dissociation of O-containing functional groups and to check the reversibility of deprotonation/protonation processes and the corresponding charge state was characterized by electrophoretic mobility measurements in parallel with colloidal stability tests. The effect of oxidative debris from SLGO synthesis on surface charging was also studied by titration and zeta potential measurement and supported by ATR-FTIR spectra of original and purified samples from suspensions at different pHs.

2. Materials and methods

2.1. Materials used

Single layer graphene oxide (SLGO) was obtained from Cheap Tubes Inc. (Cambridgeport, VT, USA) and was used both as received (referred as original, oSLGO) and after purification (referred to as pSLGO) to remove potential oxidative debris. The approximate atomic composition is C 35–42%, O 45–55% and H 3–5% and the X-ray photoelectron spectra provided by the supplier [40] indicate the presence of C═O, C—O and O–C═O type bonds besides the C—C bonds of both sp^2 and sp^3 hybridization. For purification, the oSLGO was titrated with 0.1 M KOH solution to pH ~10 and back with 0.1 M HCl solution to pH ~3 several times (3–6 times). The settled suspension was cleaned from the excess salt by washing three times with dilute HCl (pH ~ 2) and centrifuging. Finally, ultrapure water was used to wash out any chloride residual according to $AgNO_3$ test and the separated pSLGO was freeze-dried to obtain dry solid sample.

Another batch of SLGO sample was synthesized for coagulation kinetics measurements, according to the Hummers-Offeman method. 1 g of graphite (SGA-20; Kropfmühl GmbH, Germany) and 1 g of $NaNO_3$ were mixed in a flask before the addition of 30 mL of cc. H_2SO_4. This slurry was stirred and 3 × 1 g of $KMnO_4$ was added in three portions in 2 h at 50 °C, and it was kept at this temperature for another 2 h after the addition of the last portion of potassium permanganate. The reaction was terminated by adding 30 mL of ~1–2 °C water and then H_2O_2 solution (~3–4 mL) was gradually added until the suspension turned to golden brown. The acidic slurry was then centrifuged for 10 min at 3400 rpm, the supernatant was removed, the sediment was washed with water and this washing process was repeated 3–4 times. The final wet sediment was transferred to dialysis bags and dialyzed for ca. 30 days with periodic change of deionized water until its conductivity dropped below 10 μS/cm. The GO sample was then stored as aqueous suspension, the concentration of which was determined by evaporating a known mass of dispersion to air-dry state.

Graphite oxide (GO) was also prepared according to the method of Brodie [1] as detailed in [9] for the moderately oxidized batch of "GO-1" with C/O ratio of 2.56. The Brodie GO sample used in the present study is also low-oxidized and has a similar chemical composition ($CO_{0.414}H_{0.202} \times 0.0878\ H_2O$) and C/O ratio (2.42). Briefly, graphite was mixed with $NaClO_3$ and reacted with fuming HNO_3 at room temperature. After ageing for 18 h, the temperature was raised to 60 ± 1 °C and kept for 8 h. The product was transferred into water and washed several times with HCl and deionized water until the specific conductivity dropped below 10 μS/cm. The GO settled from the aqueous suspension was dried at 60 °C.

The HA was extracted from brown coal (Dudar, Hungary) by a traditional alkaline extraction procedure using 0.1 M NaOH solution and purified thoroughly [11]. The ash content of raw HA was reduced by HF/HCl treatment. The dried, ground HA was extracted with benzene/ethanol in a Soxhlet apparatus for 72 h to remove tar components. Na-humate solution was prepared from the dried HA sample dissolved it in a calculated amount of NaOH to be equivalent to the total acidity of HA measured by potentiometric titration. The HA solution was prepared by cation exchange from Na-humate solution.

Ultrapure water obtained by the Zeener Power I water purification system (Human Corporation, Seoul, South Korea) was used in all experiments. Salts, acids and bases KCl, NaCl, HCl, KOH, NaOH, and the chemicals of GO synthesis ($NaNO_3$, cc. H_2SO_4, $KMnO_4$, $NaClO_3$ HNO_3 and H_2O_2) were analytical grade reagents form Molar, Hungary.

2.2. Experimental methods

Titrations of the original HA, the as-prepared GO, the oSLGO and pSLGO samples were performed by an automatic titration system. The main components are the two automatic burettes (Dosimat 665, Metrohm AG, Switzerland), a high precision potentiometer with pH preamplifier (home-made), a combined glass pH-electrode (Radelkis, Hungary) and process control by using the GIMET1 software (home designed), as described in more detail previously [39]. The electrode was calibrated both against pH buffers (pH = 2.07, 7.10 and 9.31 of Radelkis Ltd. Hungary, RK-21, RK-71 and RK-91, respectively) and background electrolytes NaCl and KCl at three different concentrations. The potentiometer readings were correlated with the international pH-scale through buffer calibrations and with the actual proton (or hydroxide ion at pHs above 7) concentration in the medium of the titrated samples through the background electrolyte calibrations. The actual amount of protons adsorbed on or desorbed from the sample surface, i.e., the extent of proton association/dissociation (or alternatively, net surface proton excess or net proton consumption) was calculated in the course of the titrations via the proton/hydroxyl mass balance equation $n^{\sigma}_{H+/OH-} = (V/m) \times (c_{0,H+/OH-} - c_{e,H+/OH-})$. Here, V/m means volume/mass, that is, the solid to liquid phase ratio, and $c_{0,H+/OH-}$ and $c_{e,H+/OH-}$ are the proton/hydroxide ion concentrations in the solution phase after titrant addition (0.1 M HCl or 0.1 M NaOH or KOH) and after the establishment of interfacial proton equilibria, respectively. CO_2 free condition was maintained via the preparation of NaOH and KOH titrants free from CO_2, by air connecting the base titrant container through a CO_2 absorber, by frequent testing of the base titrants with hydrazine sulfate using freshly boiled ultrapure water and by applying a constant flow of N_2 in the titration vessel.

The FTIR-ATR spectra were measured in the 400–4000 cm^{-1} wavenumber range with a resolution of 2 cm^{-1} by a Bio-Rad Digilab Division

FTS-65A/896 spectrometer equipped with a Harrick's Meridian Split Pea Diamond ATR accessory. Single reflection mode was used to accumulate 256 scans for each spectrum. The background spectra were measured on the clean and dry diamond crystal. SLGO dispersions were prepared by weighing ~0.5 mg of the original or purified samples into 4 mL of 0.5 M KCl solution, the pH of which was adjusted to 3.05, 5.84, 7.15 and 9.69, respectively. One drop from the sediments of the suspensions was cast to the diamond crystal surface for the experiments.

Electrophoretic mobility (zeta potential) was measured with a Nano ZS apparatus (Malvern) in disposable zeta cells (DTS 1060). The accuracy of zeta potential measurements was ±5 mV as given by the manufacturer. The dispersion concentrations in 0.01 and 0.1 M electrolytes (NaCl and KCl media, respectively, for the HA and SLGO samples) were set to produce the optimal intensity of 105 counts per seconds. The pH of the dispersions was varied between pH ~2 and ~10. Ultrasound-assisted contactless stirring of the samples provided a kinetically stable state prior to the measurements. The zeta potential values were calculated by using the Smoluchowski equation.

The dynamic light scattering size measurements were performed by a Zetasizer Nano ZS apparatus (Malvern) with He—Ne laser (λ = 633 nm, max 4 mW), operating in backscattering mode at an angle of 173°. The HA and SLGO dispersions were prepared at 10 mM and 100 mM ionic strength (NaCl) and the concentrations were identical to those used in the zeta potential experiments. The pH of the samples was adjusted to values between 1 and 10.5 just before the measurements. The samples were homogenized in an ultrasonic apparatus for 10 s and the measurements were initiated after 60 s of relaxation. The intensity average (Z average) values were chosen to characterize the size of the dynamic units, calculated via the second order cumulant fit of the autocorrelation functions [41].

Coagulation kinetics were studied in dilute systems of 0.25 g/L HA and 0.001 g/L GO mass concentrations at pH = 4.5 ± 0.1 and 5 ± 0.1, respectively, at different NaCl concentrations up to 1.5 M. We measured the change in the Z_{ave} (average hydrodynamic diameter) values with time by using a Nano ZS (Malvern, UK) apparatus in backscattering alignment (scattering angle of 173°). In a typical experiment, data were collected for 15 min with a time resolution of 60 s. The polydispersity indices (PDIs) were <0.3 for HA and GO samples, except for the non-coagulating HA samples, where the PDIs increased to 0.7. Plots of the stability ratios (W) as a function of the electrolyte concentration (c_{NaCl}) in logarithmic representation were used to find critical coagulation concentrations (CCCs), which characterize the salt tolerance of the colloid systems. The stability ratio is a quantity that primarily depends on the concentration of the salt (coagulant) and reaches its maximum value of 1, when the coagulant concentration exceeds the CCC and the dispersion undergoes fast (diffusion controlled) aggregation. The latter condition was achieved at c = 1 M NaCl for Hummers-GO and 1.5 M for HA, respectively. Therefore, values of W were calculated as the initial slope of the kinetic curve ($dZ_{ave}/dt = f(t)$) measured at the highest salt concentration (1.5 M NaCl for HA and 1.0 M for GO), divided by the initial slope determined at the actual c_{NaCl} [42,43]:

$$W(c) = \frac{\lim_{t\to 0}\frac{dZ_{ave}}{dt}\ (fast)}{\lim_{t\to 0}\frac{dZ_{ave}}{dt}}(c) \quad (1)$$

3. Results and discussion

3.1. pH-dependent dissociation of acidic functionalities on HA and SLGO at different ionic strengths

The evaluation of acid-base titration results allows to calculate values of net surface proton excess ($\Delta n^{\Gamma}_{H/OH}$, mol/g), which reflect the extent of dissociation/association of protons from/to dissociable surface groups. The negative net surface proton excess of organic acids is equivalent to the amount of negatively charged groups, i.e., OH^- consumption in the deprotonation reaction of acidic, e.g., carboxylic groups (negative net proton consumption):

$$S\text{–}COOH + OH^- \Leftrightarrow S\text{–}COO^- + H_2O \quad (2)$$

or

$$S\text{–}COOH + H_2O \Leftrightarrow S\text{–}COO^- + H_3O^+ \quad (3)$$

where S stands for the surface atom to which the acidic moiety is linked, carbon in this case. The net proton consumption vs. pH curves representing the pH dependent charging behaviour of HA and pSLGO at various ionic strengths are shown in Fig. 2. The main characteristics of the deprotonation process are found to be similar for the studied materials according to the following aspects:

(i) the original pH of the purified samples is around pH = 3;
(ii) the order of magnitude of the titratable groups at pH = 10 is the same for HA (4–5 mmol/g) and SLGO (2.8–4 mmol/g) being one order of magnitude higher than that of common sparingly soluble colloidal metal oxides [44], but substantially smaller than that of highly charged polyelectrolytes such as poly(acrylic acid), which is fully deprotonated at pH = 10 [45] and carries ca. 13.9 mmol/g carboxylate groups, as calculated from its molecular structure;
(iii) there is a small but characteristic hysteresis between the up (towards higher pHs) and down (the reverse branch) parts of cyclic titration results obtained by the addition of base and acid titrants, respectively;
(iv) the ionic strength dependence of the net proton consumption of pSLGO is very similar to that of HA;

and dissimilarity is only revealed in terms of the

(v) small, but clearly distinguishable hump for the curves of HA at around pH = 6, while the curves of pSLGO are completely featureless.

The probable reason of hysteresis is that conformational changes of the relatively rigid carbon skeleton are slow and deprotonation from the originally more compact structure of HA and SLGO (weakly charged at low pH) is somewhat retarded as compared to the titration from opposite direction, i.e., the protonation of the originally open structure (highly charged at high pHs) [14,15]. The ionic strength dependence of protonation/deprotonation of HA is studied exhaustively [46]. The parallel shift in the curves is due to the increased electrostatic charge compensation caused by the increased concentration of background electrolyte.

Comparison of the proton consumption data at constant pH reveals that, in general, the screening effect should also become more pronounced with increasing surface charge density, similarly to the case of sparingly soluble metal oxide colloids and polyelectrolytes [44,45]. However, the pH-dependence of charge screening cannot be observed in the case of HA titrations and it is also very weak in the SLGO titrations. The almost complete independence of charge screening on the surface charge density can be explained by the non-uniform charging of both materials due to their chemical heterogeneity (see Fig. 1). Contrary to oxides and polyelectrolytes, the local charge density of HA and SLGO can adjust to pH changes since, with opening of the skeleton with increasing pH, charges originally forming a local electrostatic double layer can move away from each other thereby disrupting the continuous potential field.

The presence of discontinuous and heterogeneous surface potential fields and the pH-dependent conformational changes of SLGO

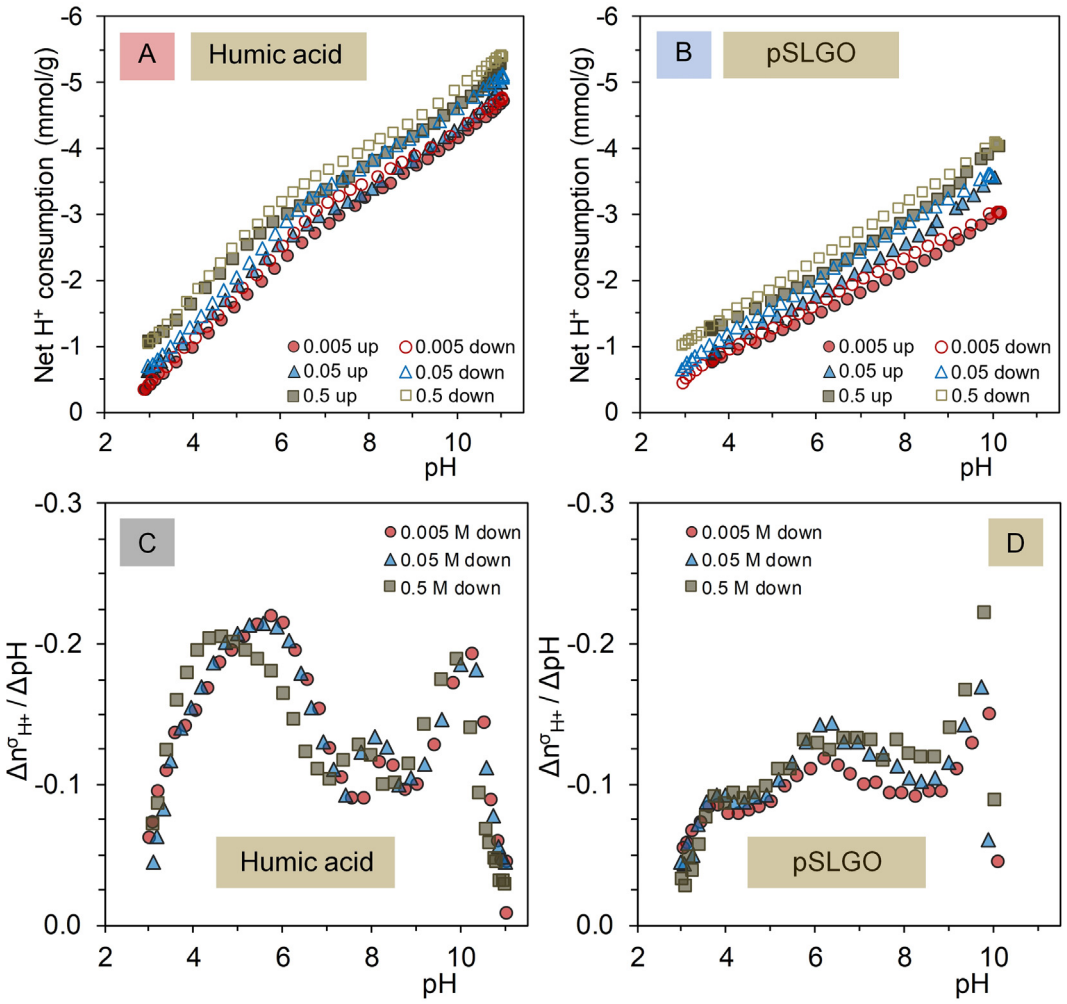

Fig. 2. Top: (A) pH-dependent dissociation of the acidic moieties of HA and (B) pSLGO measured at different ionic strengths as a function of increasing (up) and decreasing (down) pH. The sign "–" indicates proton release, i.e., the formation of negative charges. Bottom: Derivative net proton consumption vs. pH curves of (C) HA and (D) pSLGO.

nanosheets have been modelled in molecular dynamic and ab initio simulations [15]. This behaviour is close to the behaviour of connected polyelectrolyte gels and thus, the Donnan model has been successfully applied to describe the ionic strength dependence of charging of HA materials [47]. Master curves of HA titrations have also been derived to separate the electrostatic effect from the deprotonation processes [48].

In order to demonstrate the effect of the relatively flexible carbon skeleton on the charging of SLGO, we titrated the same way a graphite oxide sample prepared by the Brodie protocol, which disperses less readily in water and may remain partially delaminated (multilayered) in non-alkaline media [43]. The net surface proton excess vs. pH curves of this sample (Supporting Fig. S1A) possesses the same type of pH-dependence as other solid surfaces with variable surface charges [49], as indicated by the clearly observable divergence of the curves, in contrast to the typical, parallelly running charging curves for polyelectrolytes. Thus, an important assertion can be established in the dispersion state of the GO particles in aqueous electrolyte solutions: the determination of the charging curves at least at two different salinities can indirectly indicate if a fraction of particles exists in a multi-layered state without the need of e.g. direct thickness distribution evaluation by tedious atomic force microscopy measurements.

Finally, it is worth mentioning that, especially in the low pH-range, the net proton consumption values are much higher for the pSLGO sample (Fig. 2B), than for Brodie graphite oxide (Supporting Fig. S1A). This observation is well explained by the presence of covalent sulfate groups [50] for any samples, the synthesis protocol of which (Staudenmaier, Hummers-Offeman or any of their modifications) involved sulfuric acid. The covalent sulfates, thus, contribute additionally to the integral acidity of the pSLGO sample, in contrary to Brodie-GO, which lacks any sulfurous reagents upon its synthesis.

The heterogeneous structure of SLGO sheets has been demonstrated in scanning tunnelling and high-resolution transmission electron microscopic studies as well [51,52]. Unoxidized islands of ordered hexagonal lattice of graphene can decorate the oxidized amorphous regions in a random fashion and nanometric holes that result from the "overoxidation" of graphite may also be present. Oxidation, in essence, leads to ruptures in the lattice order.

Differentiation of the featureless protonation/deprotonation curves of HA and SLGO can be used to estimate the most probable types of dissociable groups (see in Fig. 2C, D and Supporting Fig. 1B). The peak intensities of the differentials are related to the amount of carboxyl groups with conditional (i.e., ionic strength dependent) pK_a values at the corresponding pHs. The down curves obtained during the protonation of highly negatively charged and expanded HA and SLGO were appropriate for evaluation, while the differentials of the up curves (deprotonation of weakly charged and collapsed HA and SLGO) gave scattered results (not shown here). The latter behaviour reflects also the sterically hindered deprotonation as compared to the equilibrated process of protonation of freely accessible sites. The gross charging

curves of HA (Fig. 2A) suggest the presence of two separate dissociable groups, generally assigned to –COOH and phenolic –OH, respectively [53]. The pK_a values of HA (Fig. 2C) are in the range of 4–6 (carboxylic groups) and 10–11 (phenolic OH groups). An additional characteristic peak appears at pH ~8 independently of ionic strengths that can be assigned to the acid-base equilibrium of N-containing heterocycles. The spread of the pK_a values of –COOH groups between pH 4 and 6 can be explained by the differences in the local molecular environment of the individual carboxylic moieties. The ionic strength dependence of the derivative curves in this range shows that the increase in charge screening shifts the pK_a values by more than one pH unit.

Although the charging of SLGO seems to be fully nonspecific with no hint of separate pK_a values (Fig. 2B), differentiation reveals a broad but well-discernible peak and a shoulder in the net surface proton excess vs. pH curves (Fig. 2D). The broad peak refers to a wide distribution of pK_a values between ~5 and ~8, resembling to that of the carboxylic groups of HA although ionic strength dependence is not observed in this case. The shoulder at pH 3.5–4, which is also independent of the ionic strength, is completely absent from the derivative of HA charging curves. This peak is hardly associated with carboxylic groups, but its pK_a of ~3.8 is also relatively far from the negative logarithm of the second dissociation constant of sulfuric acid ($pK_{a,2} = 2.0$). However, we think that the assignment as a sulfate half-ester is still more likely because the organosulfate groups are expected to exhibit an acidic strength similar to that of a HSO_4^- anion. This assumption is also supported by the fact that the derivative charging function of Brodie-GO (Supporting Fig. S1B) does not have any indication of this shoulder at low pHs, but only shows a carboxylate-related peak between pH 4 and 7. In conclusion, acid-base titrations of both SLGO and graphite oxide suggest the presence of Brønsted acidic centers in large quantities, which is contrary to the commonly accepted picture that the acidic groups are located primarily at the edges but not on the planes of the nanosheets [34,35,54,55] as it is suggested in [36] for phenolic groups.

Comparing the acid–base titration results of non-purified and purified SLGO samples, we found that some weakly acidic-type organic debris was removed by the applied procedure because the large step in the down curves in the range of pH ~6.5 to ~5.5 was minimized (see in Figs. 3A and 2B). The hysteresis loops between the up and down titrations were also reduced and the remaining loops were stable during further up and down titration cycles of pSLGO. This is a strong experimental argument against the suggestions of Dimiev et al. [8] that single layered graphene oxide materials would be chemically unstable in aqueous medium and that they would undergo irreversible degradation during acid-base titrations.

The net negative charge of the SLGO sample at pH ~10 decreased by ~0.5–1.0 mmol/g due to purification (Fig. 3B). This suggests the presence of a considerable amount of acidic impurity in oSLGO. The presence of impurity in graphene oxide materials as oxidative debris is widely accepted and purification is performed mainly by washing the as-prepared (acidic) samples with water [16,35,56]. As it can be deduced from our titration results, however, it is impossible to eliminate all impurities in this way. In order to access all the removable small molecules, the graphene oxide sheets should be fully unfolded by increasing the pH to ~10. Our purification procedure was successful, because before washing with water, the alkaline solution was applied and the impurities from the open SLGO sheets could be removed completely. Faria et al. [55] also applied 0.1 M NaOH solution to SLGO nanosheets and obtained chemically pure material. The definite dependence of the purification efficiency on pH and the stable residual hysteresis between the up and down titration curves support the earlier results of modelling conformational changes of SLGO sheets [15].

3.2. FTIR characterization of the functional moieties of SLGO

To shed more light and find spectroscopic indication of the presence of carboxyl functional groups, FTIR-ATR spectra were taken in function of pH of both the oSLGO and pSLGO samples (Fig. 4). The original spectra were shifted to zero absorbance value in the range of 1900–1800 cm^{-1} (no absorption of infrared radiation) and normalized relative to the heights of the characteristic bands at 1597 cm^{-1}. Normalization was necessary because the amount of SLGO dried from aqueous dispersion on the surface of the diamond crystal was different and uncontrollable.

The spectra of oSLGO (Fig. 4A) featured several characteristic absorption bands in the mid-wavelength IR region: 1726 cm^{-1} (–C=O stretching), 1367 cm^{-1} (symmetric carboxylate $–COO^-$ stretching), 1246 cm^{-1} (comprised of a mixture of C—O stretch and C–O–H bend), and finally one peak at 1597 cm^{-1}. The latter is a complex band, to which several vibration modes may contribute: νC=C skeletal band of aromatic domains, β_{OH} of water and ν_{as} of COO^-. This overlap of the asymmetric carboxylate stretching with the signal of adsorbed H_2O molecules, does not allow for clarification of its dissociation state. However, this evaluation can be unambiguously performed by considering the ν_s of COO^- peak and the peak of the carbonyl stretch. Accordingly,

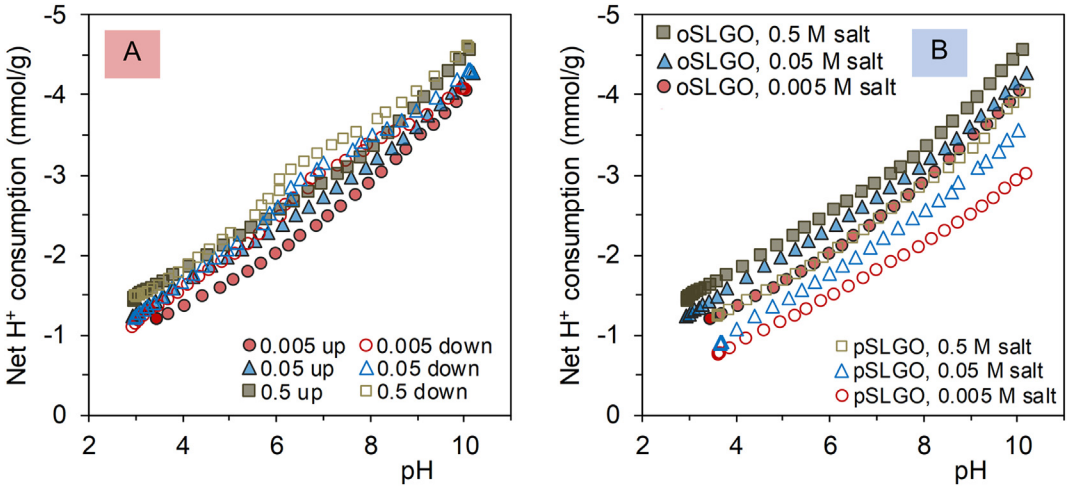

Fig. 3. (A) The hysteresis loops between the two parts of the cyclic titration curves: towards higher pHs ("up") and the return run towards decreasing pHs ("down") of the oSLGO sample at three different ionic strengths of 5; 50 and 500 mM, and (B) the decrease in the amounts of the acidic groups of the SLGO sample as a result of purification seen as the downshift in the net proton consumption vs. pH curves of pSLGO as compared to oSLGO.

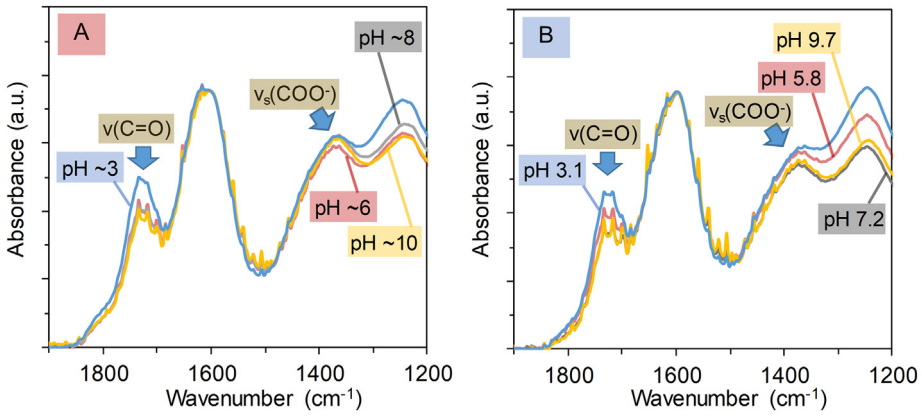

Fig. 4. FTIR-ATR spectra of (A) oSLGO and (B) pSLGO samples measured at different pHs.

the absorbance of the band of the protonated form at 1726 cm^{-1} was divided by that of the asymmetric carboxylate at 1367 cm^{-1} to obtain the ratio denoted as α, which is plotted as a function of pH in Supporting Fig. S2. Remarkably, the peak ratio gradually decreased with the pH, giving a spectroscopic evidence of the carboxylic groups that undergo base-induced dissociation. However, it is noteworthy that the 1726 cm^{-1} peak has not disappeared even at pH > 10, where most of the carboxylic groups are expected to be dissociated. This is a clear indication, in line with our earlier DRIFT study on Brodie graphite oxide [57], that SLGO involves carbonyl structural motifs which are not sensitive to pH changes; such as those in isolated ketone, quinone or enone (alkene conjugated to ketone) groups.

Regarding the purified (pSLGO) sample, it yields absorption bands corresponding to the same wavenumbers as found for oSLGO (Fig. 4B). No remarkable changes were observed in the peak intensities either; the absorbance ratios of carboxylate-related bands fall close to that of the original sample as shown in Supporting Fig. S2. While the possibility of the removal of some highly carboxylated carbonaceous fragments cannot be ruled out by FTIR, it confirms that the pSLGO is decorated by a considerable amount of COOH groups, and the purification process has not influenced the ratio of different types of functional groups of GO.

3.3. pH-dependent charge state and colloidal stability of HA and SLGO

The electrophoretic mobility (electrokinetic potential) measurement results are demonstrated in Fig. 5A and B. The zeta potential of both HA and pSLGO is negative all over the studied pH range, which indicates the presence of excess negative charges even at very low pH values in harmony with the titration results (Figs. 2 and 3). The negative zeta potential values could originate not only from acidic dissociation of functional groups with low pK_a values, but also from permanent negative charges embedded in the skeletal structure (such as in the case of clay minerals [58] and other cation exchangers [59]), which are unresponsive to acid/base addition and thus are undetectable by titration but can be detected by electrokinetic measurements. However, the fact that the titration-derived charging curves and the zeta potential-pH functions simultaneously start from slightly negative values and then their absolute values increase in the same manner clearly implies that permanent negative charges are absent from both HA and GO. It is important to highlight the parallelism between the pH-dependencies of the ζ-potentials of these materials (absolute values at the same pH and ionic strength are slightly greater for HA), which also supports the striking similarity of pSLGO and humic acids. This is in full harmony with their charging properties quantified as the net proton consumption in acid-base titrations, e.g., ~5 mmol/g and ~4 mmol/g for HA and pSLGO, respectively, at the highest pH values measured and I = 0.5 M (Fig. 2). The effect of purification of SLGO on the pH dependence of zeta potential is seen by contrasting with the oSLGO in Fig. 5B. With increasing pH, the electrokinetic potential of the oSLGO is significantly higher (in absolute value) than that of the purified sample (compared at 10 mM ionic strength), indicating the presence of highly carboxylated carbonaceous fragments in the unpurified material.

At low pHs (<3–4), the amount of the negative charge from dissociated, anionic forms of strongly acidic sites is not sufficient to keep the dispersions in colloidally stable state, as indicated by the values of zeta potential to be less than ~−30 mV at the ionic strength of our experiments (I = 10 and 100 mM). In general, ±~25 mV is the limit of colloidal stabilization in aqueous media. As the pictures in Fig. 5 (bottom panel) indicate, HA becomes fully stabilized above pH = 1 at low salt concentrations and even at pHs > 2 in 100 mM NaCl. Regarding SLGO, it also remains dispersed in progressively increasing quantities from low to high pHs, at 10 mM ionic strength. In high-salt environment, however, only a small fraction of the SLGO platelets remain suspended, but most of them settle down in one day. One might assume that this separation of particles is the result of particle aggregation. However, a suspension may also exhibit sedimentation in the absence of coagulation, if the dispersed objects are large enough that the gravitational pull overcomes their thermal motion. To shed more light on this issue, dynamic light scattering measurements were performed to determine the pH-induced changes in the hydrodynamic diameters of HA and SLGO particles. For HA, Fig. 5C shows that the particle size is around 200 nm independently of the salt concentration, but it abruptly increases to 800 nm by lowering the pH from 2 to 1, resulting in the settling of precipitated HA. For CheapTube's SLGO, the Z-average diameters were found to be always larger than 1000 nm (Fig. 5D). Clearly, an aggregation occurs for this sample even under moderately acidic conditions, which is unexpected for this material regarding its widely considered superior dispersion properties. It is likely that the weaker dispersibility is caused by both the purification process and the low oxidation degree of this batch.

Finally, it is worth noting that even in the solution of greater salinity, a small amount of GO sheets remained suspended between 2 < pH < 8. This observation is explained by the large polydispersities (PDI = 0.52 at 10 mM; and 0.44 at 100 mM NaCl) which well substantiate the assumption that the SLGO particles are not aggregated at intermediate pHs, but the large-sized fractions completely sediment after 1 day of standstill. The in-depth characterization of the electrolyte tolerance will then be described in the next section.

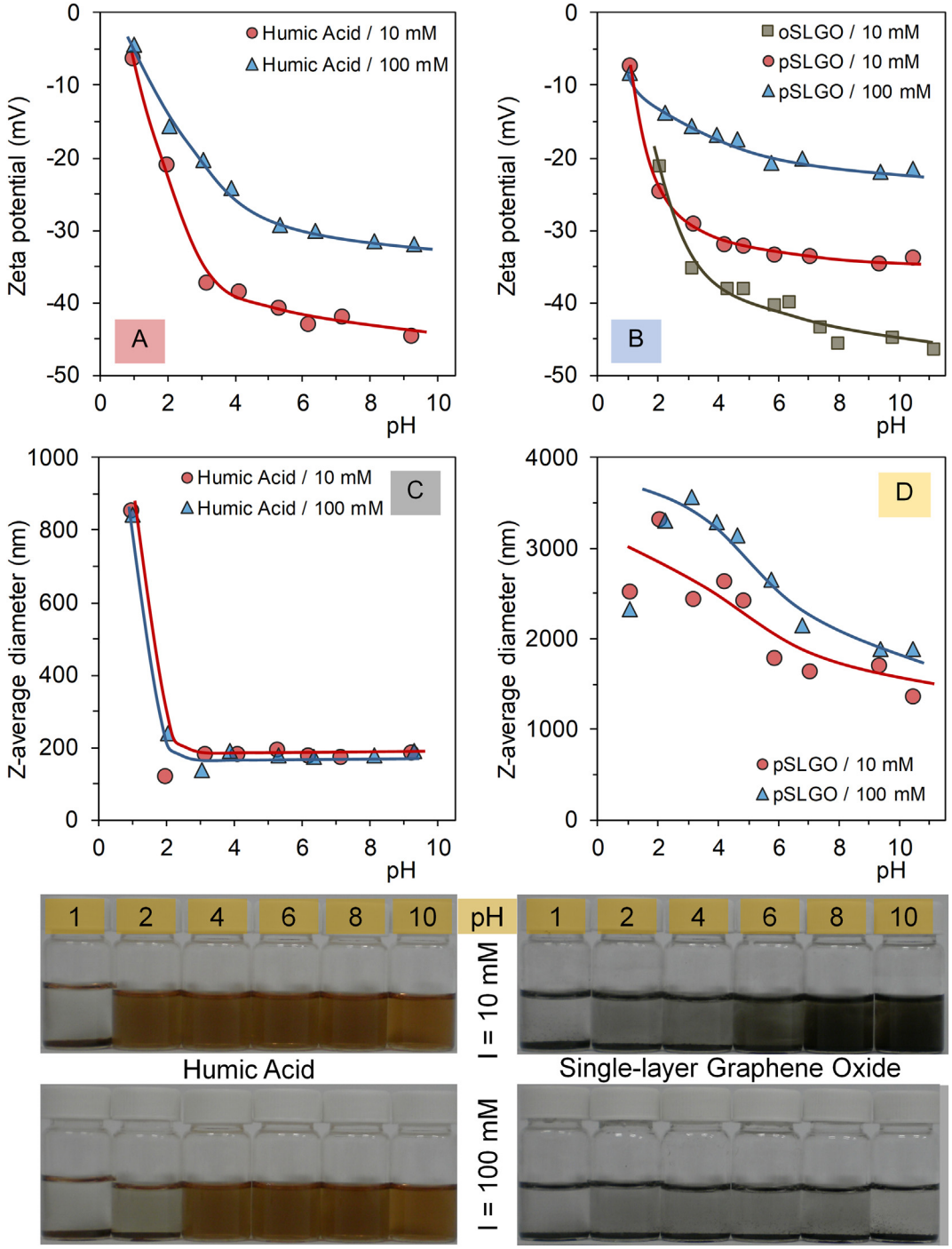

Fig. 5. pH-dependent charge state of HA and SLGO characterized by measuring (A, B) electrophoretic mobility (zeta potential) and (C, D) hydrodynamic diameter (Z average data) at 100 mM and 10 mM NaCl concentrations. The pictures show the sedimentation of the dispersions after standing for 1 day at increasing pH values between 1 and 10 at 10 and 100 mM ionic strengths.

3.4. Salt tolerance of HA and GO at constant pH

Time-resolved coagulation kinetic measurements were performed to characterize the colloidal stability of HA and GO in aqueous NaCl solutions under slightly acidic condition. The size evolution of aggregates in time was followed by dynamic light scattering. Fig. 6A and B shows the size evolution in pure HA solutions and SLGO sols at different salt concentrations. The traditional term 'sol' is used here to distinguish the particles of 410 nm initial diameter (obtained from own synthesis) used for this salt tolerance test from the large, micron-sized platelets (obtained from Cheap Tubes) used for description of the pH-dependence of zeta potential (Fig. 5). The slope of kinetic curves (Z-average diameter versus time functions) is proportional to the coagulation rate [60]. These slopes increase with increasing amount of added NaCl in the range of slow coagulation, above which it becomes independent of the salt concentration, when fast coagulation (diffusion limited aggregation) takes place. The initial part of the curves in Fig. 6 was used for further analysis. Coagulation kinetics were measured up to 1.5 M and

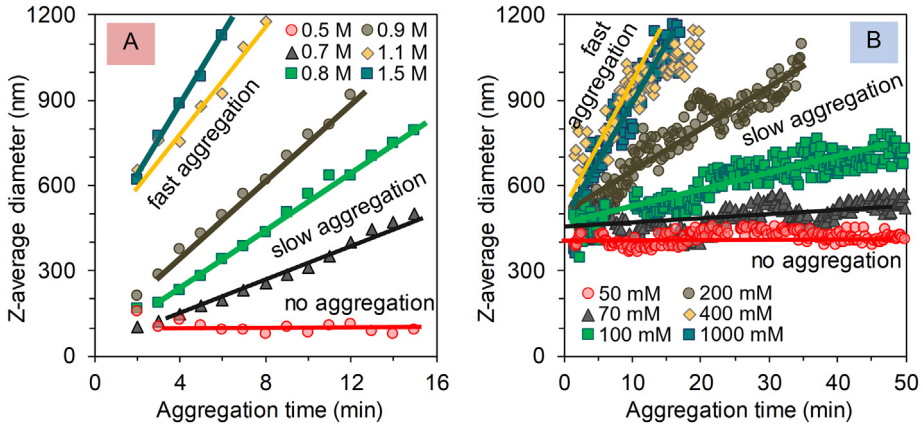

Fig. 6. Coagulation kinetics measured by dynamic light scattering: the size evolution of aggregates in the (A) HA and (B) SLGO systems at pH 4.5 ± 0.2 and 5.5 ± 0.2, respectively, at different NaCl concentrations and 25 ± 0.1 °C.

1.0 M NaCl in pure HA and GO systems at pH 4.5 ± 0.2 and 5.5 ± 0.2, respectively. Stability ratios (W) were calculated according to Eq. (1) as suggested in literature [61,62]. The critical coagulation concentration (CCC) can be determined from the stability plots [60] as the lowest concentration value at which W equals to 1, as shown in Fig. 7.

For HA, as shown in Fig. 7, the CCC is ~1 M. Such a high value is indicative of highly charged macromolecules which are not destabilized by the extensive charge screening provided by the highly saline medium. The aggregation slows down below this concentration, and no precipitation occurs below ca. 600 mM ionic strength. On the contrary, 400 nm SLGO particles obtained by the Hummers method undergo fast aggregation above the CCC of 300 mM. This peculiar difference must be explained not only by an associated difference in the charge density of HA (~2 mmol/g at pH ~4.5, $I = 0.5$ M) and the surface charge density of GO (~1.5 mmol/g at pH ~5.5, I = 0.5 M), but by the difference in the size of the initial, non-aggregated particles. We have recently demonstrated the substantial size dependence of the CCCs for graphene oxides [43]. In that publication, the CCC of a Brodie graphite oxide of 450 nm hydrodynamic diameter was 80 mM. The present SLGO sample has approximately the same size (Z_{ave} = 410 nm) but its CCC is four times higher, which can be explained by its larger surface charge density. For multi-layered micron-sized graphite oxides, the CCC is ca. 50 mM, and this difference in salt tolerance is even larger. Therefore, in respect to their aggregation in weakly acidic media, Hummers-SLGO represents a closer analogy with HA than with its structurally and chemically analogous counterpart, Brodie-graphite oxide.

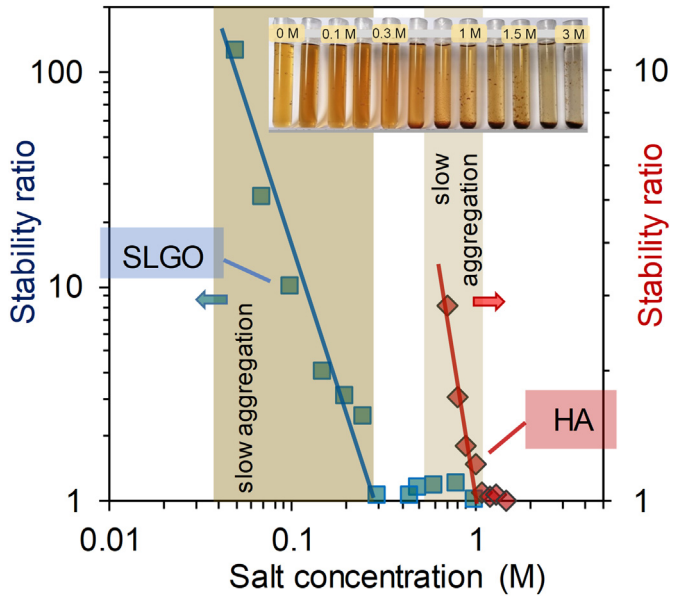

Fig. 7. Stability plots for aqueous HA and Hummers-GO systems in NaCl solutions at pH 4.5 ± 0.2 and 5.5 ± 0.2, respectively. The shaded areas represent the concentration regions where slow aggregation takes place. Stable systems are observable at lower salts, while the right hand side of the shaded area delineate the respective CCCs (280 mM for GO; 1.0 M for HA). The inserted photograph shows the effect of increasing NaCl concentration up to 3 M on the colloidal stability of HA solutions (picture was taken after 1 day of rest); the partial aggregation of polydisperse HA and dark sediments of aggregated parts are visible at concentrations >0.5 M.

4. Conclusion

This paper presents a novel investigation involving in-depth evaluation and comparative study of two, strikingly similar carbonaceous materials, humic acid and graphene oxide, mostly focusing on their colloid chemical behaviour. Besides the striking analogy between the acidic dissociation of single-layer graphene oxide and HA, it turned out that their charging characteristics definitely differ from that of graphite oxide. While the charging curves of multilayered GO particles diverge from each other at higher pHs, the net H^+ consumption vs. pH curves of the exfoliated counterpart and HA run parallel, which is characteristic for the charging of rigid but ionisable macromolecules.

In equilibrium acid base titration, all three substances showed hysteresis loops probably due to the conformational changes of carbon skeletons, which are small for the more flexible SLGO and HA samples reaching a reversible polyelectrolyte-like behaviour, but large for rigid multilayer GO. The latter shows characteristic particle-like behaviour similarly to the opening charge-potential curves of metal oxides [39]. The reversibility of the surface charge curves clearly demonstrates the absence of any chemical degradation occurring for GO within the studied time frame (3–5 h) and pH window. Based on experimental proofs delicate details of SLGO purification were revealed. The surface charging, colloidal stability, adsorption propensities have remarkably changed after accurate cleaning. The colloidal stability of HA is generally much better than that of different GO samples. Probably the latter and the very good adsorption ability of HA are the reason for the recent observation that the electrolyte tolerance of different GO materials is considerably increased in the presence of dissolved humic substances [63]. This enhanced colloidal stability is highly desirable e.g. for transport of engineered GO nanoparticles in environment, and the use of HA as surface modifier for GO membranes [64] or for preparation of high-tech GO composite materials for printed electrodes [65].

CRediT authorship contribution statement

Etelka Tombácz: Conceptualization, Data curation, Writing - original draft, Writing - review & editing. **Ildikó Y. Tóth:** Investigation,

Formal analysis, Funding acquisition. **Krisztina Kovács:** Investigation, Formal analysis. **Erzsébet Illés:** Methodology, Funding acquisition. **Márta Szekeres:** Methodology, Validation, Data curation, Writing - original draft. **Balázs Barna:** Investigation. **Attila Csicsor:** Investigation. **Tamás Szabó:** Formal analysis, Visualization, Writing - original draft, Writing - review & editing, Funding acquisition.

Declaration of competing interest

There is no conflict of interest among authors to report this work.

Acknowledgements

Project no. 126498 has been implemented with the support provided from the National Research, Development and Innovation Fund of Hungary, financed under the KH funding scheme. The financial supports by the János Bolyai Research Scholarship of the Hungarian Academy of Sciences and by the Ministry of Human Capacities, Hungary through the grant ÚNKP-19-4 New National Excellence Program are gratefully acknowledged. The support from the Open Access Fund of the University of Szeged (No. 4590) is also acknowledged. The graphite sample used for the SLGO synthesis was a gift from Graphit Kropfmühl GmbH, Germany.

Appendix A. Supplementary data

Supplementary data to this article can be found online at https://doi.org/10.1016/j.molliq.2020.112948.

References

[1] B.C. Brodie, On the atomic weight of graphite, Philos. Trans. R. Soc. Lond. 149 (1859) 249–259.
[2] W.S. Hummers Jr., R.E. Offeman, Preparation of graphitic oxide, J. Am. Chem. Soc. 80 (1958) 1339, https://doi.org/10.1021/ja01539a017.
[3] M. Estévez, R. Juan, C. Ruiz, J.M. Andrés, Formation of humic acids in lignites and subbituminous coals by dry air oxidation, Fuel 69 (1990) 157–160, https://doi.org/10.1016/0016-2361(90)90166-N.
[4] M.H.B. Hayes, Concepts of the origins, composition, and structures of humic substances, in: W.S. Wilson (Ed.), Advances in Soil Organic Matter Research: The Impact on Agriculture and the Environment, Special Publication No. 90, The Royal Society of Chemistry, Thomas Graham House, Science Park, Cambridge, England 1991, pp. 3–22.
[5] M.H.B. Hayes, P. MacCharty, R.L. Malcolm, R.S. Swift, Humic substabces II, Search of Structure, John Wiley and Sons, New York, 1989.
[6] M. Schnitzer, S.U. Khan, Humic Sustances in the Environment, Marcel Decker Inc., New York, 1972.
[7] H. Thiele, Über salzbildung und basenaustausch der graphitsäure, Kolloid-Zeitschrift 80 (1937) 1–20, https://doi.org/10.1007/BF01518573.
[8] A.M. Dimiev, L.B. Alemany, J.M. Tour, Graphene oxide. Origin of acidity, its instability in water, and a new dynamic structural model, ACS Nano 7 (2013) 576–588, https://doi.org/10.1021/nn3047378.
[9] G. Huang, W. Kang, Q. Geng, B. Xing, Q. Liu, J. Jia, C. Zhang, One-step green hydrothermal synthesis of few-layer graphene oxide from humic acid, Nanomaterials 8 (2018), 215. https://doi.org/10.3390/nano8040215.
[10] H. Pallmann, Dispersoidchemische probleme in der humusforschung, Kolloid-Zeitschrift 101 (1942) 72–81, https://doi.org/10.1007/BF01519968.
[11] E. Tombácz, Colloidal properties of humic acids and spontaneous changes of their colloidal state under variable solution conditions, Soil Sci. 164 (1999) 814–824.
[12] E. Tombácz, E. Meleg, A theoretical explanation of the aggregation of humic substances as a function of pH and electrolyte concentration, Org. Geochem. 15 (1990) 375–381, https://doi.org/10.1016/0146-6380(90)90164-U.
[13] T. Szabó, E. Tombácz, E. Illés, I. Dékány, Enhanced acidity and pH-dependent surface charge characterization of successively oxidized graphite oxides, Carbon 44 (2006) 537–545, https://doi.org/10.1016/j.carbon.2005.08.005.
[14] R.L.D. Whitby, A. Korobeinyk, V.M. Gun'ko, R. Busquets, A.B. Cundy, K. Laszlo, J. Skubiszewska-Zięba, R. Leboda, E. Tombácz, I.Y. Toth, K. Kovacs, S.V. Mikhalovsky, pH-driven physicochemical conformational changes of single-layer graphene oxide, Chem. Commun. 47 (2011) 9645–9647, https://doi.org/10.1039/C1CC13725E.
[15] R.L.D. Whitby, V.M. Gun'ko, A. Korobeinyk, R. Busquets, A.B. Cundy, K. László, J. Skubiszewska-Zieba, R. Leboda, E. Tombácz, I.Y. Tóth, K. Kovács, S.V. Mikhalovsky, Driving forces of conformational changes in single-layer graphene oxide, ACS Nano 6 (2012) 3967–3973, https://doi.org/10.1021/nn3002278.
[16] H. Kerndorff, M. Schnitzer, Sorption of metals on humic acid, Geochim. Cosmochim. Acta 44 (1980) 1701–1708, https://doi.org/10.1016/0016-7037(80)90221-5.
[18] S. Chowdhury, R. Balasubramanian, Recent advances in the use of graphene-family nanoadsorbents for removal of toxic pollutants from wastewater, Adv. Colloid Interf. Sci. 204 (2014) 35–56, https://doi.org/10.1016/j.cis.2013.12.005.
[19] R.R. Amirov, J. Shayimova, Z. Nasirova, A.M. Dimiev, Chemistry of graphene oxide. Reactions with transition metal cations, Carbon 116 (2017) 356–365, https://doi.org/10.1016/j.carbon.2017.01.095.
[20] A.N. Solodov, J. Shayimova, R.R. Amirov, A.M. Dimiev, Binding modes of Fe (III) with graphene oxide in aqueous solutions. Competition with Sr^{2+}, Cs^{+}, Na^{+} ions and Fe (III) chelators, J. Mol. Liq. 302 (2020), 112461. https://doi.org/10.1016/j.molliq.2020.112461.
[21] T. Kuila, S. Bose, A.K. Mishra, P. Khanra, N.H. Kim, J.H. Lee, Chemical functionalization of graphene and its applications, Prog. Mater. Sci. 57 (2012) 1061–1105, https://doi.org/10.1016/j.pmatsci.2012.03.002.
[22] T. Kuilla, S. Bhadra, D. Yao, N.H. Kim, S. Bose, J.H. Lee, Recent advances in graphene based polymer composites, Prog. Polym. Sci. 35 (2010) 1350–1375, https://doi.org/10.1016/j.progpolymsci.2010.07.005.
[23] J. Liu, L. Cui, D. Losic, Graphene and graphene oxide as new nanocarriers for drug delivery applications, Acta Biomater. 9 (2013) 9243–9257, https://doi.org/10.1016/j.actbio.2013.08.016.
[24] A.B. Bourlinos, D. Gournis, D. Petridis, T. Szabó, A. Szeri, I. Dékány, Graphite oxide: chemical reduction to graphite and surface modification with primary aliphatic amines and amino acids, Langmuir 19 (2003) 6050–6055, https://doi.org/10.1021/la026525h.
[25] A. Bakandritsos, M. Pykal, P. Błoński, P. Jakubec, D.D. Chronopoulos, K. Poláková, V. Georgakilas, K. Čépe, O. Tomanec, V. Ranc, A.B. Bourlinos, R. Zbořil, M. Otyepka, Cyanographene and graphene acid: emerging derivatives enabling high-yield and selective functionalization of graphene, ACS Nano 11 (2017) 2982–2991, https://doi.org/10.1021/acsnano.6b08449.
[26] J.A. Luceño-Sánchez, A.M. Díez-Pascual, Grafting of polypyrrole-3-carboxylic acid to the surface of hexamethylene diisocyanate-functionalized graphene oxide, Nanomaterials 9 (2019), 1095. https://doi.org/10.3390/nano9081095.
[27] J. Wang, J. Wei, S. Su, J. Qiu, Z. Hu, M. Hasan, E. Vargas, M. Pantoya, S. Wang, Thermal-recoverable tough hydrogels enhanced by porphyrin decorated graphene oxide, Nanomaterials 9 (2019), 1487. https://doi.org/10.3390/nano9101487.
[28] I. Rodriguez-Pastor, G. Ramos-Fernandez, H. Varela-Rizo, M. Terrones, I. Martin-Gullon, Towards the understanding of the graphene oxide structure: how to control the formation of humic- and fulvic-like oxidized debris, Carbon 84 (2015) 299–309, https://doi.org/10.1016/j.carbon.2014.12.027.
[29] Y. Dong, L. Wan, J. Cai, Q. Fang, Y. Chi, G. Chen, Natural carbon-based dots from humic substances, Sci. Rep. 5 (2015), 10037. https://doi.org/10.1038/srep10037.
[30] D.W. Van Krevelen, Organic geochemistry – old and new, Org. Geochem. 6 (1984) 1–10, https://doi.org/10.1016/0146-6380(84)90021-4.
[31] R.L. Sleighter, P.G. Hatcher, The application of electrospray ionization coupled to ultrahigh resolution mass spectrometry for the molecular characterization of natural organic matter, J. Mass Spectrom. 42 (2007) 559–574, https://doi.org/10.1002/jms.1221.
[32] J.A. Rice, P. MacCarthy, Statistical evaluation of the elemental composition of humic substances, Org. Geochem. 17 (1991) 635–648, https://doi.org/10.1016/0146-6380(91)90006-6.
[33] C.T. Johnston, E. Tombácz, Chapter 2: surface chemistry of soil minerals, in: J.B. Dixon, D.G. Schulze (Eds.), Soil Mineralogy With Environmental Applications, Soil Science Society of America, John Wiley and Sons, Madison, WI 2002, pp. 37–67.
[34] D.R. Dreyer, S. Park, C.W. Bielawski, R.S. Ruoff, The chemistry of graphene oxide, Chem. Soc. Rev. 39 (2010) 228–240, https://doi.org/10.1039/B917103G.
[35] A. Lerf, H. He, M. Forster, J. Klinowski, Structure of graphite oxide revisited, J. Phys. Chem. B 102 (1998) 4477–4482, https://doi.org/10.1021/jp9731821.
[36] T. Szabó, O. Berkesi, P. Forgó, K. Josepovits, Y. Sanakis, D. Petridis, I. Dékány, Evolution of surface functional groups in a series of progressively oxidized graphite oxides, Chem. Mater. 18 (2006) 2740–2749, https://doi.org/10.1021/cm060258+.
[37] G. Zhao, J. Li, X. Ren, C. Chen, X. Wang, Few-layered graphene oxide nanosheets as superior sorbents for heavy metal ion pollution management, Environ. Sci. Technol. 45 (2011) 10454–10462, https://doi.org/10.1021/es203439v.
[38] D. Gu, J.B. Fein, Adsorption of metals onto graphene oxide: surface complexation modeling and linear free energy relationships, Colloids Surf. A Physicochem. Eng. Asp. 481 (2015) 319–327, https://doi.org/10.1016/j.colsurfa.2015.05.026.
[39] M. Szekeres, E. Tombácz, Surface charge characterization of metal oxides by potentiometric acid–base titration, revisited theory and experiment, Colloids Surf. A Physicochem. Eng. Asp. 414 (2012) 302–313, https://doi.org/10.1016/j.colsurfa.2012.08.027.
[40] http://www.cheaptubes.com/product-category/graphene-oxide/ (latest open: 10.03.2020).
[41] B.J. Frisken, Revisiting the method of cumulants for the analysis of dynamic light-scattering data, Appl. Opt. 40 (2001) 4087–4091, https://doi.org/10.1364/AO.40.004087.
[42] E. Illés, E. Tombácz, The effect of humic acid adsorption on pH-dependent surface charging and aggregation of magnetite nanoparticles, J. Colloid Interface Sci. 295 (2006) 115–123.
[43] T. Szabo, P. Maroni, I. Szilagyi, Size-dependent aggregation of graphene oxide, Carbon 160 (2020) 145–155, https://doi.org/10.1016/j.carbon.2020.01.022.
[44] R.O. James, G.A. Parks, Characterization of aqueous colloids by their electrical double layer and intrinsic surface chemical properties, in: E. Matijevic (Ed.), Surface and Colloid Science, vol. 12, Plenum Press, New York 1982, pp. 119–216.
[45] M. Borkovec, B. Jönsson, G.J.M. Koper, Ionization processes and proton binding in polyprotic processes: small molecules, proteins, interfaces, and polyelectrolytes, in: E. Matijevic (Ed.), Surface and Colloid Science, vol. 16, Kluwer Academic/Plenum Press, New York 2001, pp. 99–339.

[46] C.J. Milne, D.G. Kinniburgh, J.C.M. De Wit, W.H. van Riemsdijk, L.K. Koopal, Analysis of proton binding by a peat humic acid using a simple electrostatic model, Geochim. Cosmochim. Acta 59 (1995) 1101–1112, https://doi.org/10.1016/0016-7037(95)00027-W.
[47] M.F. Benedetti, W.H. van Riemsdijk, L.K. Koopal, Humic substances considered as a heterogeneous Donnan gel phase, Environ. Sci. Technol. 30 (1996) 1805–1813, https://doi.org/10.1021/es950012y.
[48] J.C.M. De Wit, W.H. van Riemsdijk, L.K. Koopal, Proton binding to humic substances. 1. Electrostatic effects, Environ. Sci. Technol. 27 (1993) 2005–2014, https://doi.org/10.1021/es00047a004.
[49] E. Tombácz, M. Szekeres, Colloidal behavior of aqueous montmorillonite suspensions: the specific role of pH in the presence of indifferent electrolytes, Appl. Clay Sci. 27 (2004) 75–94, https://doi.org/10.1016/j.clay.2004.01.001.
[50] A. Dimiev, D.V. Kosynkin, L.B. Alemany, P. Chaguine, J.M. Tour, Pristine graphite oxide, J. Am. Chem. Soc. 134 (2012) 2815–2822, https://doi.org/10.1021/ja211531y.
[51] C. Gómez-Navarro, R.T. Weitz, A.M. Bittner, M. Scolari, A. Mews, M. Burghard, K. Kern, Electronic transport properties of individual chemically reduced graphene oxide sheets, Nano Lett. 7 (2007) 3499–3503, https://doi.org/10.1021/nl072090c.
[52] K. Erickson, R. Erni, Z. Lee, N. Alem, W. Gannett, A. Zettl, Determination of the local chemical structure of graphene oxide and reduced graphene oxide, Adv. Mater. 22 (2010) 4467–4472, https://doi.org/10.1002/adma.201000732.
[53] J.D. Ritchie, E.M. Perdue, Proton-binding study of standard and reference fulvic acids, humic acids, and natural organic matter, Geochim. Cosmochim. Acta 67 (2003) 85–96, https://doi.org/10.1016/S0016-7037(02)01044-X.
[54] Z. Guo, S. Wang, G. Wang, Z. Niu, J. Yang, W. Wu, Effect of oxidation debris on spectroscopic and macroscopic properties of graphene oxide, Carbon 76 (2014) 203–211, https://doi.org/10.1016/j.carbon.2014.04.068.
[55] A.F. Faria, D. Stéfani, T. Martinez, A.C.M. Moraes, M.E.H. Maia da Costa, E.B. Barros, A.G. Souza Filho, A.J. Paula, O.L. Alves, Unveiling the role of oxidation debris on the surface chemistry of graphene through the anchoring of Ag nanoparticles, Chem. Mater. 24 (2012) 4080–4087, https://doi.org/10.1021/cm301939s.
[56] J. Song, X. Wang, C.-T. Chang, Preparation and characterization of graphene oxide, J. Nanomater. 2014 (2014), 276143. https://doi.org/10.1155/2014/276143.
[57] T. Szabó, O. Berkesi, I. Dékány, DRIFT study of deuterium-exchanged graphite oxide, Carbon 43 (2005) 3186–3189, https://doi.org/10.1016/j.carbon.2005.07.013.
[58] W.P. Kelley, Cation exchange in soils, Monograph Series (American Chemical Society), No. 109, Reinhold Pub. Corp, New York, 1948.
[59] F. De Dardel, T.V. Arden, Ion Exchangers. Principles and Applications, Ullmann's Encyclopedia of Industrial Chemistry, Sixth edition Wiley-VCH Verlag GmbH, 2001 1–70.
[60] R.J. Hunter, Foundations of Colloid Science, vol. 1, Clarendon Press, Oxford, 1987.
[61] M. Schudel, S.H. Behrens, H. Holthoff, R. Kretzschmar, M. Borkovec, Absolute aggregation rate constants of hematite particles in aqueous suspensions: a comparison of two different surface morphologies, J. Colloid Interface Sci. 196 (1997) 241–253, https://doi.org/10.1006/jcis.1997.5207.
[62] H. Holthoff, S.U. Egelhaaf, M. Borkovec, P. Schurtenberger, H. Sticher, Coagulation rate measurements of colloidal particles by simultaneous static and dynamic light scattering, Langmuir 12 (1996) 5541–5549, https://doi.org/10.1021/la960326e.
[63] Y. Jiang, R. Raliya, P. Liao, P. Biswas, J.D. Fortner, Graphene oxides in water: assessing stability as a function of material and natural organic matter properties, Environ. Sci.: Nano 4 (2017) 1484–1493, https://doi.org/10.1039/C7EN00220C.
[64] T.J. Konch, R.K. Gogoi, A. Gogoi, K. Saha, J. Deka, K.A. Reddy, K. Raidongia, Nanofluidic transport through humic acid modified graphene oxide nanochannels, Mater. Chem. Front. 2 (2018) 1647–1654, https://doi.org/10.1039/C8QM00272J.
[65] Y.M. Shulga, S.A. Baskakov, Y.V. Baskakova, A.S. Lobach, E.N. Kabachkov, Y.M. Volfkovich, V.E. Sosenkin, N.Y. Shulga, S.I. Nefedkin, Y. Kumar, A. Michtchenko, Preparation of graphene oxide-humic acid composite-based ink for printing thin film electrodes for micro-supercapacitors, J. Alloys Compd. 730 (2018) 88–95, https://doi.org/10.1016/j.jallcom.2017.09.249.